PERGAMON

International Journal of Heat and Mass Transfer 43 (2000) 1089–1102

International Journal of HEAT and MASS TRANSFER

www.elsevier.com/locate/ijhmt

A visual study of phase-change heat transfer in a two-dimensional porous structure with a partial heating boundary

Q. Liao, T.S. Zhao*

Department of Mechanical Engineering, The Hong Kong University of Science and Technology, Clear Water Bay, Kowloon, Hong Kong

Received 10 December 1998; received in revised form 15 June 1999

Abstract

A visual study on the phase-change behaviors in a vertical two-dimensional porous structure made of staggered miniature silver–copper circular cylinders has been carried out. Subcooled water was pumped into the porous structure from its bottom due to the capillary action developed in the vicinity of a grooved heating block placed on the top of the porous structure. Using a high-speed video imaging system, both pore-scale bubble-growth behaviors and continuum-scale distributions of two-phase zone in the porous structure were observed. Photographic results reveal that for a small or moderate heat flux, isolated bubbles formed, grew, and collapsed in the pores in a cyclic manner with a nearly constant frequency. In the macroscopic view, it is found that the periodic downflows of dispersed bubbles and upflows of the liquid phase in the porous structure led to a quasi-steady liquid–vapor two-phase zone. As the imposed heat flux was increased, both the frequency of the bubble growth–collapse cycle and the number of isolated bubbles increased while in the macroscopic view, the two-phase zone expanded laterally but shrank vertically. When the imposed heat flux was sufficiently high, a vapor film was observed beneath the heated fin. These visual observations explain heat transfer measurements: with an increase of the imposed heat flux, the heat transfer coefficient increases to a maximum value and then rapidly decreases afterwards.

Keywords: Phase-change heat transfer; Porous media; Boiling; Inverted meniscus evaporator

1. Introduction

Problems involving phase-change heat transfer in porous media with a vertical or a horizontal bounding heated surface have been studied extensively in the past because of their important technological applications [1]. In this work, we consider the problem of boiling heat transfer in a porous structure heated with a permeable boundary; a porous structure is heated from a grooved heating block placed on its top, as schematically shown in Fig. 1. Interest in this topic arose from the growing efforts on the development of a so-called 'inverted meniscus' type evaporator [2–5]. This innovative evaporator is a key component of miniature flat heat pipes [5], capillary pumped loops (CPL) and loop heat pipes which are widely used for cooling of electrical and electronic devices [6,7] as well as for the thermal management of advanced space platforms and military spacecraft [8].

Some analytical and numerical studies on the heat

* Corresponding author. Tel.: +852-2358-8647.
E-mail address: metzhao@ust.hk (T.S. Zhao).

0017-9310/00/$ - see front matter
PII: S0017-9310(99)00212-4

Nomenclature

A_h	total cross-sectional area, m^2
h	heat transfer coefficient of evaporator, $W/m^2/K$
ΔH	adverse hydrostatic head, m
q''	heat flux, kW/m^2
Q	heat transporting from heating block to porous structure, W
T	temperature, K
$\bar{T}_w$	mean temperature of the heating block, K

Subscripts

s	saturation
w	heating block

Superscripts

-	mean value
$''$	flux

transfer characteristics of the inverted meniscus type evaporators have been reported. Wulz and Embacher [9] theoretically studied a flat-plate evaporator using a steady state two-dimensional model accounting for the dry region in the porous matrix. By prescribing the location of the liquid–vapor interface and the interface temperature, they studied the liquid flow and heat transfer in the porous region. Cao and Faghri [10,11] described the physical mechanisms of the evaporator of CPLs and identified possible limits related to the evaporator operation. In another paper, Cao and Faghri [11] numerically simulated a flat-plate type evaporator by solving a conjugate heat transfer problem including three sub-domains: subcooled liquid flow and heat transfer in the porous structure, three-dimensional vapor flow in the groove, and the heat conduction in the cover plate. The liquid and vapor flows were coupled via the interfacial mass flux. Demidov and Yatsenko [12] numerically investigated the heat and mass transfer processes during evaporation in a wet capillary structure with a rectangular grooved heated wall. One of the important assumptions they made was: there existed a superheated vapor zone in the vicinity of the heated groove tip as well as a liquid meniscus near the corners formed by the lateral sides of the fin of the heating block and the top surface of the porous structure. When the vapor zone expanded beyond the surface of the heated wall, this liquid meniscus would disappear. They concluded that the critical heat flux was reached when the expansion of the vapor zone exceeded the area of the heated surface. Khrustalev and Faghri [5] investigated the heat and mass transfer processes around a heated triangular solid fin penetrating into a wetted porous structure. They also assumed that the heated surface and the wet porous media is separated by a vapor film. Based on this assumption, they concluded that the critical heat flux for this particular configuration was reached (1) when the increase of the thermal resistance between the heated surface of the fin and the liquid zone with increasing heat flux lead to an extremely high temperature which is unacceptable in practice, or (2) when the thickness of the vapor zone around the fin tip was equal to the thickness of the porous structure. However, the assumption of the presence of the vapor film between the heated surface and the subcooled liquid has never been experimentally confirmed.

Relatively few experimental data on the heat transfer characteristics of the inverted meniscus type evaporators are available in the literature. Deng et al. [13] experimentally investigated the heat transfer coefficient and the critical heat flux of the inverted meniscus evaporators consisting of steel screens with various meshes. Most recently, Liao and Zhao [14] conducted an experimental investigation on the capillary-driven heat and mass transfer processes in a vertical rectangular capillary porous structure of glass beads with a grooved heating boundary at the top. Their experimental results show that as the imposed heat flux was increased, the heat transfer coefficient was first increased to a maximum value and then decreased afterward. A further increase in the imposed heat flux lead to the occurrence of the boiling crisis, reflected by a rapid rise in both the heating block and the outlet vapor temperatures.

Most of the previous investigators have focused on the studies of the performance characteristics of the inverted meniscus type evaporators. However, some crucial mechanisms related to the phase-change behaviors in the porous structure adjacent the heated surface remain elusive. For instance, the information of the distribution of liquid and vapor phases in a porous structure is needed for the development of an accurate prediction of the heat transfer coefficient and the critical heat flux of the inverted meniscus type evaporators. However, visualization of multiphase flows through a packed-sphere bed is a rather difficult task because the porous medium is often constructed by spheres in a typical experiment. The difficulty in obtaining distinct imaging of various phases remains even if the porous medium is consisting of transparent solids beads. This is because transparent beads refract light and the curved fluid-solid interfaces make light paths quickly randomized, and flow imaging is impossible. For this

reason, a number of tools for the visualization of multiphase flows through a porous medium have been developed. Examples include computed tomography [15,16] nuclear magnetic resonance [17], electromagnetic tomography [18], and microwave attenuation [19]. However, each of these methods for measuring saturation or bubble behaviors within laboratory cells is limited in spatial or temporal resolution or in size of the sample, or requires extremely expensive equipment.

In this paper, a visual study on the phase-change behaviors in a vertical porous structure with a partial heating and evaporation boundary at the upper surface is reported. For the purpose of flow visualization, a two-dimensional porous structure made of staggered miniature silver–copper circular cylinders was constructed. Phase-change behaviors within the porous structure were visualized via its front transparent plate using a high-speed video system. Both pore-scale bubble-growth behaviors and continuum-scale distributions of two-phase zone in the porous structure were observed. Photographic results reveal that for a small or moderate heat flux, isolated bubbles formed, grew, and collapsed in the pores in a cyclic manner with a nearly constant frequency. In the macroscopic view, it is found that the periodic downflows of dispersed bubbles and upflows of the liquid phase in the porous structure led to a quasi-steady liquid–vapor two-phase zone. As the imposed heat flux was increased, both the frequency of the bubble growth–collapse cycle and the number of isolated bubbles increased while in the macroscopic view, the two-phase zone expanded laterally but shrank vertically. When the imposed heat flux was sufficiently high, vapor film was observed beneath the heated fin. These visual observations are useful for the interpretation of the heat transfer measurements of the inverted meniscus type evaporators. It is also of significance for the development of a phenomenological model predicting the heat transfer coefficient and the critical heat flux of this type evaporator.

2. Experimental

The experiment was performed in the experimental apparatus shown in Fig. 1, which consisted of two major assemblies: the liquid supply system and the test section. The liquid supply system is described elsewhere [14]. The deionized water draining from the water tank was bifurcated into two streams in the water-level controller: one stream was directed toward the test section while the remainder was directed toward the overflow container. As such, the water level in the water-level controller could be kept constant during the experiments. The adverse hydrostatic head ΔH (the distance between the top of the porous structure and the water level) was controlled by adjusting the elevation of the platform lifter, on which the water-level controller was placed. A RTD controller with a 1.0-kW heater was installed to keep the fluid temperature in the water-level controller to a desired value. Both the water tank and the overflow container were placed on a digital scale such that the mass flow rate flowing to the test section could be measured by reading the mass change per unit time.

The test section is schematically illustrated in Fig. 2. A vertically-oriented two-dimensional porous structure with a surface area of 50×24 mm^2 was made of a number of staggered silver–copper cylinders (2.0 mm in diameter) which were inserted in a bakelite plate. The other sides of the porous structure were enclosed by two side walls (made of bakelite) and a transparent front wall (made of glass), 10 mm away from the rear plate. A heating assembly consisting of a Teflon shell and a copper grooved block was mounted on the top

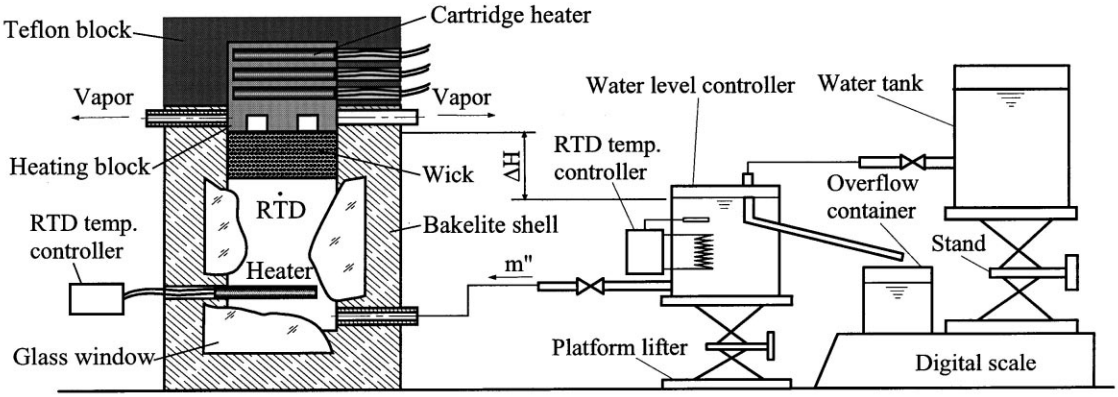

Fig. 1. Schematic of the experimental apparatus.

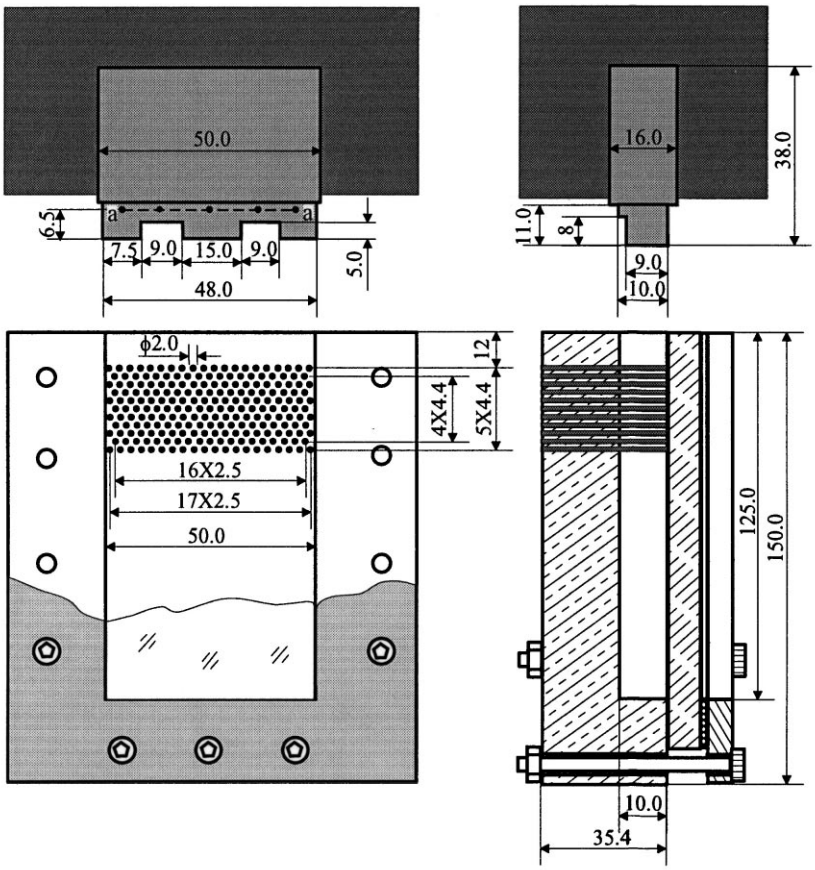

Fig. 2. Detailed design of the test section.

of the porous structure. Three 130-W heaters were installed in the heating block to provide the heating power. Special care was taken to ensure the heating block was in good contact with the top surface of the porous structure. Owing to the capillary force generated at the liquid–vapor interface near the heated surface, the subcooled liquid was induced to enter the test section from its bottom and flowed upward by overcoming the gravity and the drag forces in the porous medium. Vapor, produced near the heated surface, vented into the grooves and exited to the ambient via the vapor tube. The inlet temperature of liquid water was well controlled by a RTD temperature controller with a 50-W heater located in the lower portion of the test section.

Five T-type thermocouples of 0.8 mm in diameter were used to measure the temperatures of the heating block, while four T-type thermocouples of 0.8 mm in diameter were used for measuring the inlet liquid temperature and outlet vapor temperature of the porous structure. A data acquisition system, consisting of a personal computer, an A/D converter board (MetraByte DAS-20), and two universal analog input multiplexers (MetraByte EXP-20), was used to record temperature measurements.

A Kodak Ekapro-1000 motion analyzer, with a speed of 1000 frames/s or 6000 partial frames/s, was used to capture images of phase-change behaviors in the porous structure. Two procedures were followed to collect the visual information. In the first procedure, the camera equipped with a microscopic lens was focused on the microscopic view (see Fig. 3) to visualize the bubble behaviors in the pore level of the porous structure. In the second procedure, the camera was focused on the macroscopic view (see also Fig. 3) to observe the phase-change behaviors in the continuum scale.

In the present study, the heat transfer coefficient is defined as

$$h = \frac{Q}{A_h(\bar{T}_w - T_s)}, \tag{1}$$

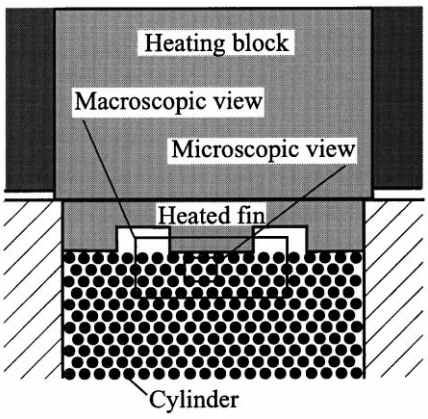

Fig. 3. View scopes of the high speed camera.

where Q is the heating power and A_h denotes the heating surface area, i.e., the cross-sectional area of the copper block. In Eq. (1), T_s is the temperature of the saturated vapor at the exit and $\bar{T}_w$ is the mean temperature of heating block which was obtained by averaging the readings of the thermocouples located along the top of grooved block (a–a), as illustrated in Fig. 3.

In order to stabilize the boiling conditions and degas the air from the porous structure, prior to each experiment, the water level of the water-level controller was adjusted slightly to the top of the porous structure and a moderate heat flux was applied at the top of porous structure for 2 h to keep water at its boiling temperature. Then, the water level was adjusted to the required elevation. For each test case, it took about 0.5–1 h for the system to be stabilized. The experimental data were collected under steady state conditions.

The three physical parameters measured during the experiments were: the temperatures of the heating block and of the liquid at inlet and vapor at outlet, the mass flux of water, as well as the imposed heating load. The thermocouples were calibrated to ensure the accuracy within $\pm 0.2^{\circ}C$. It was estimated that the uncertainty of the mass flux was $\pm 0.4\%$ while the uncertainty of the imposed heat loading was $\pm 9.5\%$, which was caused primarily by the heat loss. Using the uncertainty estimation method of Kline and McClintock [20], it was estimated that the uncertainty of the heat transfer coefficient was $\pm 12.5\%$.

3. Results and discussion

Experiments were carried out by increasing the heat flux from 16 to 322 kW/m^2 under the conditions of two different inlet temperatures (50 and 80°C) and two adverse hydrostatic heads (10 and 15 mm). In the following, the heat transfer measurements and the photographic results are presented to show the effects of the imposed heat flux, the inlet temperature of subcooled liquid, and the adverse hydrostatic heads on heat transfer behaviors for the porous structure with a periodically bounded heating boundary.

3.1. Effect of heat flux

A typical variation of the heat transfer coefficient, as defined in Eq. (1), versus the imposed heat flux for $\Delta H = 10$ mm and at $T_{li} = 50^{\circ}C$ is presented in Fig. 4. It is seen that the heat transfer coefficient increases with the increase of heat flux for small and moderate heat fluxes. When the heat flux was increased to a certain value, however, the heat transfer coefficient reached a peak value and then dropped rapidly to a point marked by 'E', where the critical heat flux was reached. This behavior is generally in agreement with the results in our previous work [14] in which glass beads were used as the porous medium. In the subsequent paragraphs, we shall focus on discussing the mechanisms leading to the heat transfer behavior shown in Fig. 4 based on the visual observations of bubble behaviors in both the microscopic and macroscopic views. Photographic results will be presented for four selected heat fluxes: $q'' = 36.99$, 109.32, 171.1, and 211.56 kW/m^2, as labeled, respectively, by letters of A, B, C, and D in Fig. 4.

Consecutive snapshots of a typical bubble lifetime during its growth and collapse cycle at a low heat flux ($q'' = 36.99$ kW/m^2, marked by 'A' in Fig. 4) for $\Delta H = 10$ mm and $T_{li} = 50^{\circ}C$ are presented in Fig. 5. These images were obtained when the high-speed camera was focusing on the microscopic view (see Fig. 3). As designated, in all these gray-scale images, the white corresponds to the solid phase (cylinders), the dark corresponds to the wet phase (liquid water), and the in-between gray scales with high luminance are the bubbles. The first frame (Fig. 5(a)) identifies an isolated bubble within the scope of view in its earlier stage of growth, where it is seen that the bubble was generated adjacent to the heated surface. A comparative scrutiny of Fig. 5(b)–(e) allows a clear picture that the bubble grew downwards and laterally along the pore space due to higher vapor pressure near the heated fin. As time further went by, two growing fronts appeared (see Fig. 5(f)) and the bubble further expanded. When the size of the bubble became sufficiently large (see Fig. 5(g)) such that its front reached the fin groove or was condensed by subcooled liquid below, a rather fast bubble collapse process began, as indicated in Fig. 5(h)–(j). Immediately following the bubble collapse, the pore space was re-occupied by replenished liquid due to the capillary action. Starting from a small bubble as shown in Fig. 5(j), another cycle of bubble growth and collapse was subsequently

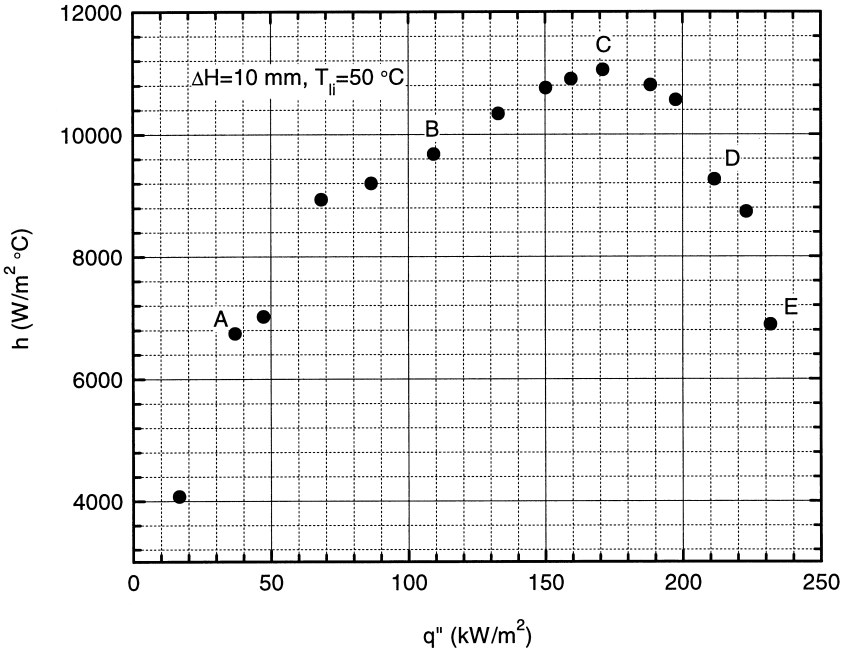

Fig. 4. Variation of the heat transfer coefficient versus the imposed heat flux.

followed. It was found that such a cyclic process of bubble growth and collapse underwent in a frequency as high as 3.33 Hz at this particular imposed heat flux ($q'' = 36.99$ kW/m^2). Under the identical experimental condition, when the high-speed camera was focused on the macroscopic view (see Fig. 3), it was found that such a high-frequency cyclic process of the bubble growth–collapse and liquid replenishment behaviors virtually led to a vapor–liquid co-existing zone, i.e., a two-phase zone, as evident from Fig. 10(a).

Next, we present the visual results at a higher heat flux $q'' = 109.32$ kW/m^2 marked by 'B' in Fig. 4. The bubble behaviors in the microscopic view are shown in Fig. 6. At higher heat fluxes, it was observed that for a single bubble, the behaviors of a single bubble were more or less the same as those for a lower heat flux presented in Fig. 5. However, it is seen from Fig. 6 that for a higher heat flux the number of isolated bubbles within the same scope of view were increased from one to two and the cyclic process of the bubble growth and collapse underwent faster, reflected by the increase of frequency from 3.33 to 8.07 Hz. In the macroscopic view, a comparison between Fig. 10(a) and (b) for low and high heat fluxes shows that the two-phase zone became wider horizontally but thinner vertically when the imposed heat flux was increased.

When the imposed heat flux was further increased to $q'' = 171.10$ kW/m^2 (marked by 'C' in Fig. 4), it is seen from Fig. 7 that the bubble growth–collapse process became much faster, reflected by a higher frequency of 13.9 Hz. It is also observed from Fig. 7 that the generated bubbles did not expand downwards as much as for the cases of low heat fluxes as shown in Figs. 5 and 6. Instead, the bubbles grew mostly horizontally towards the vapor grooves. In the macroscopic view shown in Fig. 10(c), it is obvious that the two-zone became significantly thinner in the vertical direction. This can be explained as follows. Based on the overall energy balance, the induced mass flux of the working fluid was increased with the increase of the heat flux. Thus, more subcooled liquid was moving toward the heated surface at higher heat fluxes. Because more bubbles in the two-phase zone was condensed into liquid, the depth of the two-phase zone became thinner.

The visual results at the above three selected heat fluxes (point A, B, and C in Fig. 4) indicates that as the imposed heat flux was increased, the number of primary bubbles increased and the cyclic process of the bubble growth–collapse became faster. These are the primary reasons why the heat transfer coefficient increased with the increase of the imposed heat flux for low and moderate heat fluxes.

As the imposed heat flux was increased past point C, the heat transfer coefficient decreased as shown in Fig. 4. This behavior can be explained based on the photographic results presented in Fig. 8 for $q'' = 211.56$ kW/m^2 (point D in Fig. 4). Scrutiny of Fig. 8(a) and (b) indicates that the primary bubbles coalesced immediately once they were generated from the

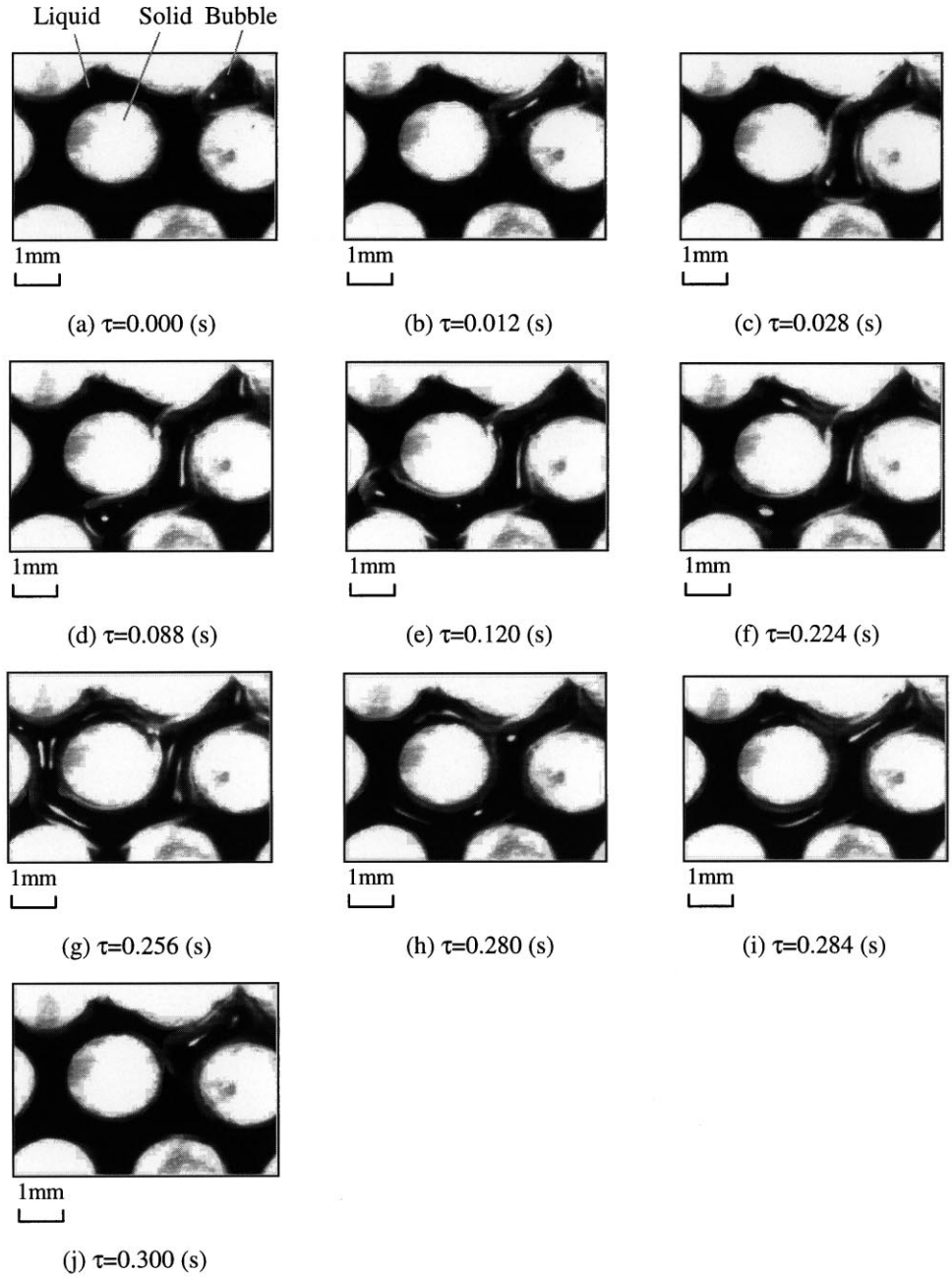

Fig. 5. Images of the bubbles in the porous structure at the imposed heat flux of 36.99 kW/m^2 for $T_{li} = 50$°C and $\Delta h = 10$ mm.

heated surface. The existence of the coalesced bubbles beneath the heated surface is one of the main features of the bubble behaviors for high heat fluxes as compared with the cases of low heat fluxes. As shown in Fig. 8(b)–(d), the coalesced bubbles remained most of time during the cycle. Once the bubbles were collapsed, another cycle followed up immediately (Fig. 8(e)). The decrease in the heat transfer coefficient for this higher heat flux can be mainly attributed to the fact that the coalesced bubbles remained beneath the heated surface most of the time during the bubble grow–collapse cycle and the liquid replenishment became harder under this situation.

As the imposed heat flux exceeded point E ($q'' =$

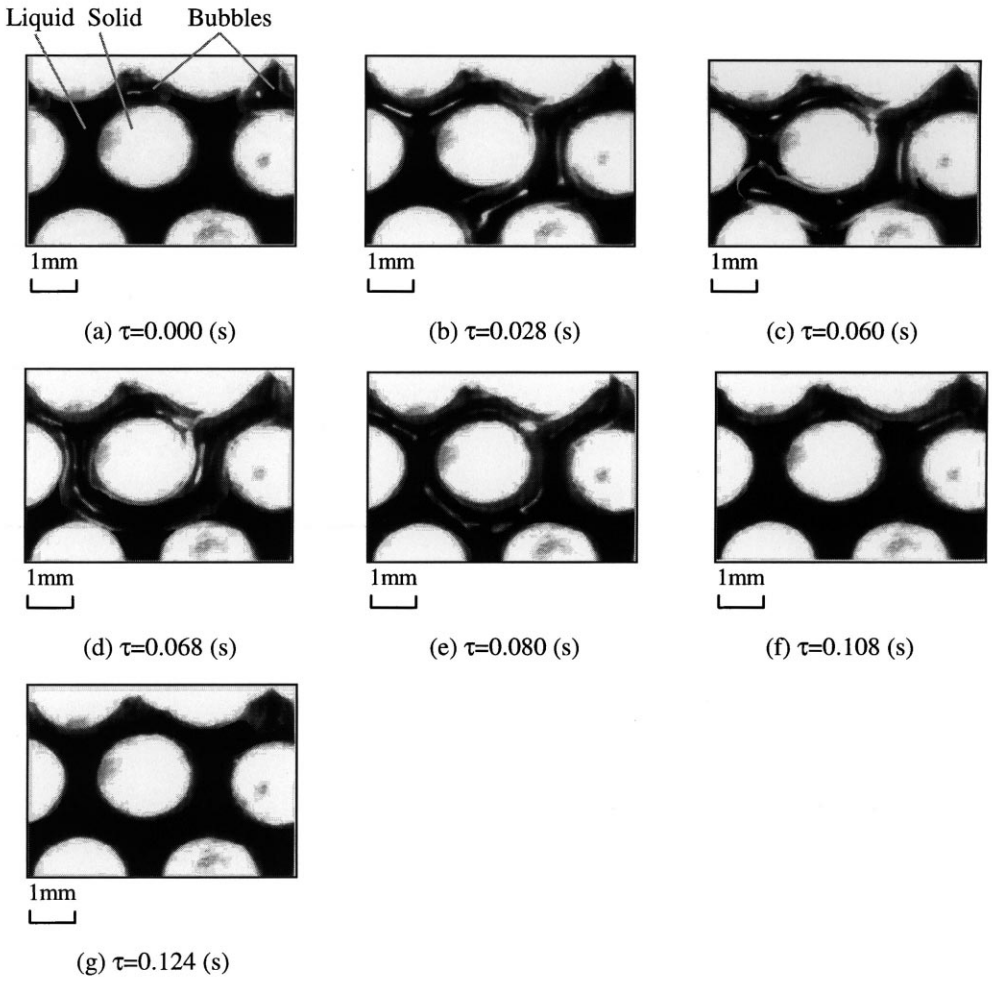

Fig. 6. Images of the bubbles in the porous structure at the imposed heat flux of 109.32 kW/m^2 for $T_{li} = 50^\circ$C and $\Delta h = 10$ mm.

231.82 kW/m^2), the coalesced bubbles beneath the heated surface for the case of point D became a stable vapor film, as presented in Fig. 9(a). Due to the lower thermal conductivity of vapor, the thermal resistance between the heated surface and the porous structure increased rapidly as the vapor film became thicker (see Fig. 9(b)). Under this situation, it was found that both the wall and the outlet temperatures increased exponentially and the steady state condition could not be maintained anymore.

Based on our visual observations for lower and moderate heat fluxes, we can conclude that a two-phase zone existed in the porous structure adjacent to the heated surface and this two-phase zone expand laterally and shrank vertically as the imposed heat flux was increased (see Fig. 10). Correspondingly, the heat transfer coefficient increased with the increase of heat flux until a peak value occurred. At a sufficiently high heat flux, the coalesced bubbles caused an increase in the thermal resistance between the heated surface and the porous structure, resulting in a rapid drop in the heat transfer coefficient with the increase of heat flux. When the imposed heat flux exceeded the critical heat flux, a stable vapor film was formed underneath the heated surface, thereby the temperatures both in the heating block and in the vapor exit increasing rapidly.

3.2. Effect of inlet temperature

The effect of the inlet temperature of the subcooled liquid on the heat transfer coefficient for two adverse hydrostatic heads ($\Delta H = 10$ and 15 mm) is illustrated in Fig. 11(a) and (b), respectively. These two figures show that the inlet temperature of subcooled liquid has substantial influence on the heat transfer performance, a higher inlet temperature leading to both higher

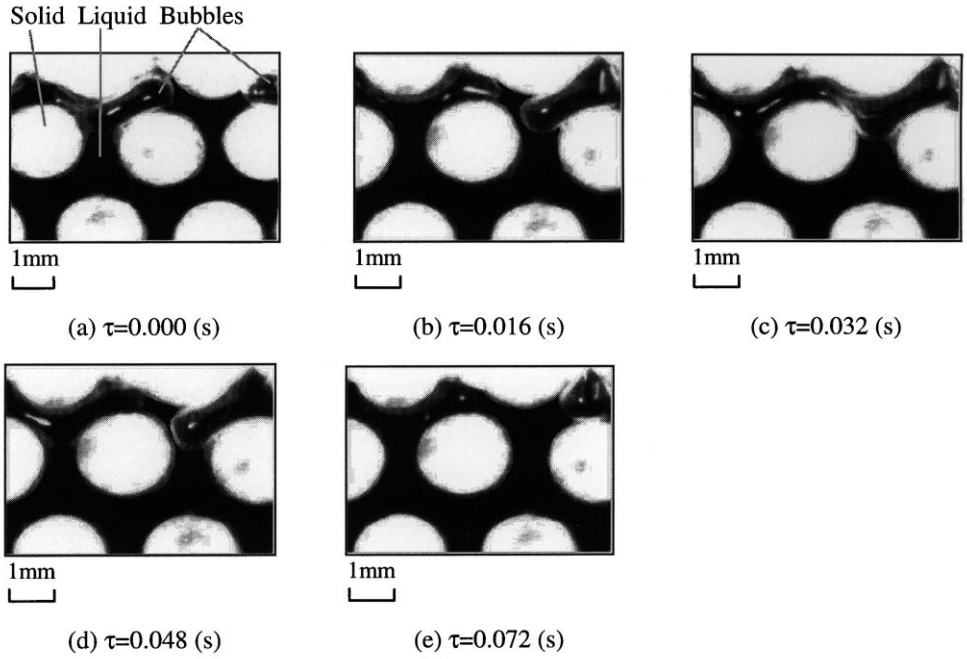

Fig. 7. Images of the bubbles in the porous structure at the imposed heat flux of 171.10 kW/m^2 for $T_{li} = 50°C$ and $\Delta h = 10$ mm.

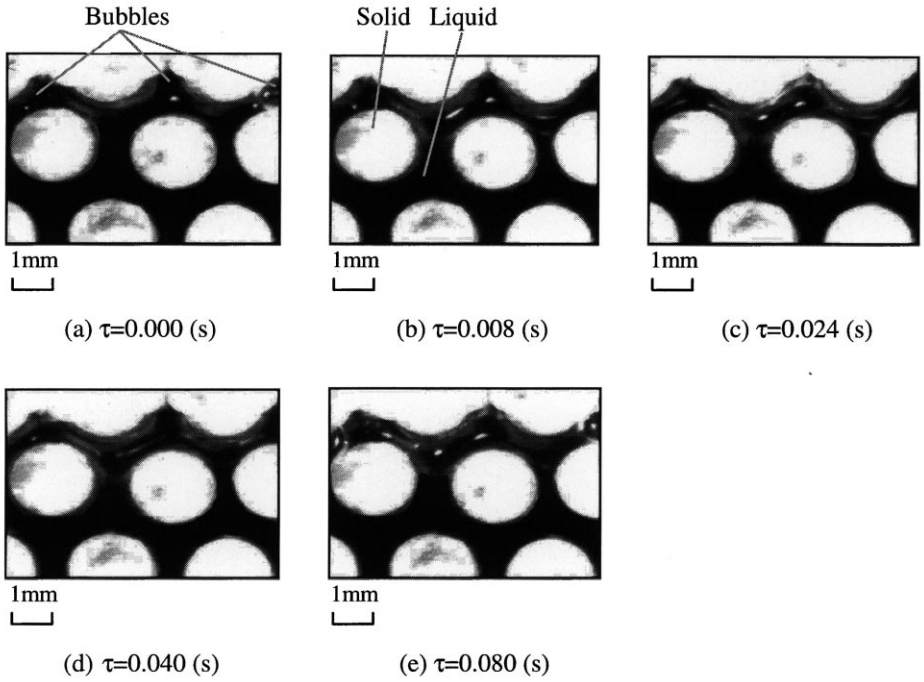

Fig. 8. Images of the bubbles in the porous structure at the imposed heat flux of 211.56 kW/m^2 for $T_{li} = 50°C$ and $\Delta h = 10$ mm.

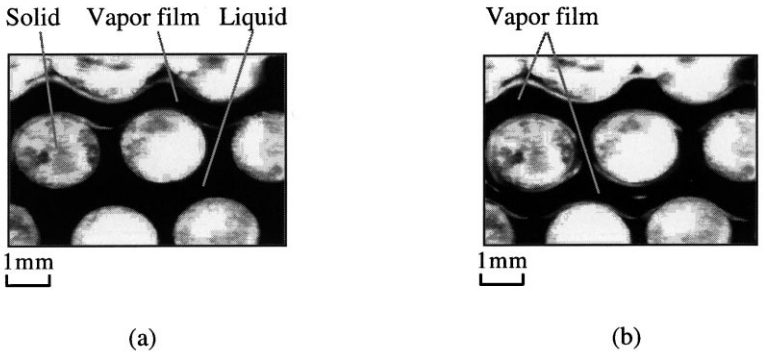

Fig. 9. Images of the vapor film in the porous structure at the imposed heat flux of 236.69 kW/m^2 for $T_{li} = 50$°C and $\Delta h = 10$ mm.

heat transfer coefficient and critical heat flux. In order to explain the influence of the inlet temperature of the subcooled liquid on the heat transfer performance, we present the photographic results of bubble behaviors in the macroscopic view for almost the same heat flux ($q'' = 109.32$ and 110.83 kW/m^2) at two different inlet temperatures (50 and 80°C) in Fig. 12(a) and (b). A comparison between Fig. 12(a) and (b) indicates that the two-phase zone (the region where bubbles and liquid coexist) became wider in the horizontal direction for a higher inlet temperature (Fig. 12(b)). This is because that when the inlet temperature is closer to the saturated value, more nucleate sites will be created. As such, a wider two-phase zone was maintained for a higher inlet temperature of the subcooled liquid. A larger evaporation surface provided by a larger two-phase zone will significantly enhance heat and mass transfer between the grooved heating block and the porous

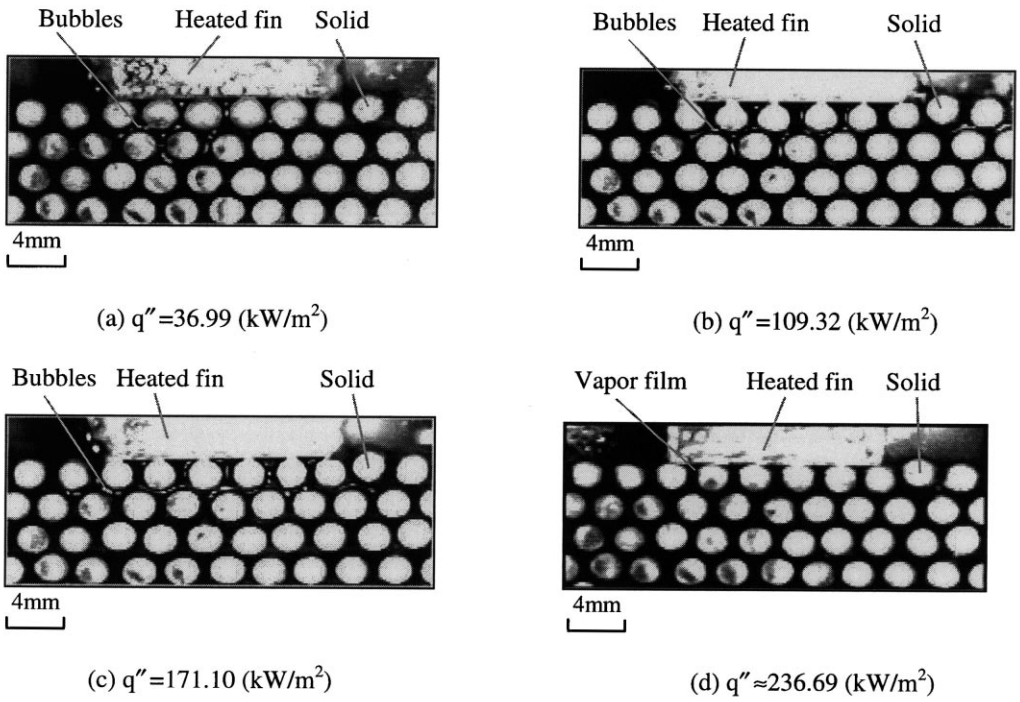

Fig. 10. Images of the two-phase zone below the heated surface for $T_{li} = 50$°C and $\Delta h = 10$ mm.

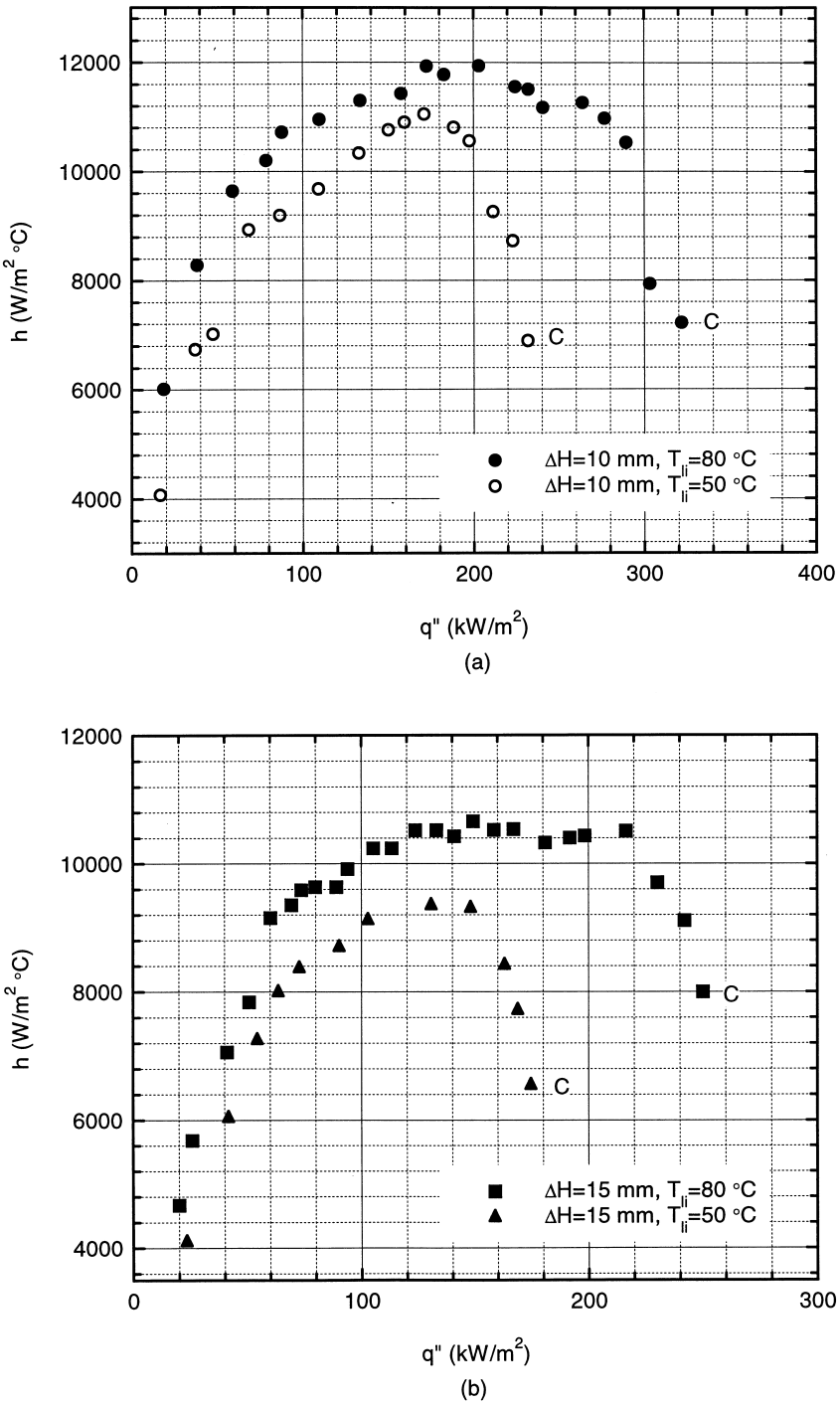

Fig. 11. Effect of the inlet temperature on the heat transfer coefficient at $\Delta h = 10$ and 15 mm (where 'C' represents the critical heat flux point).

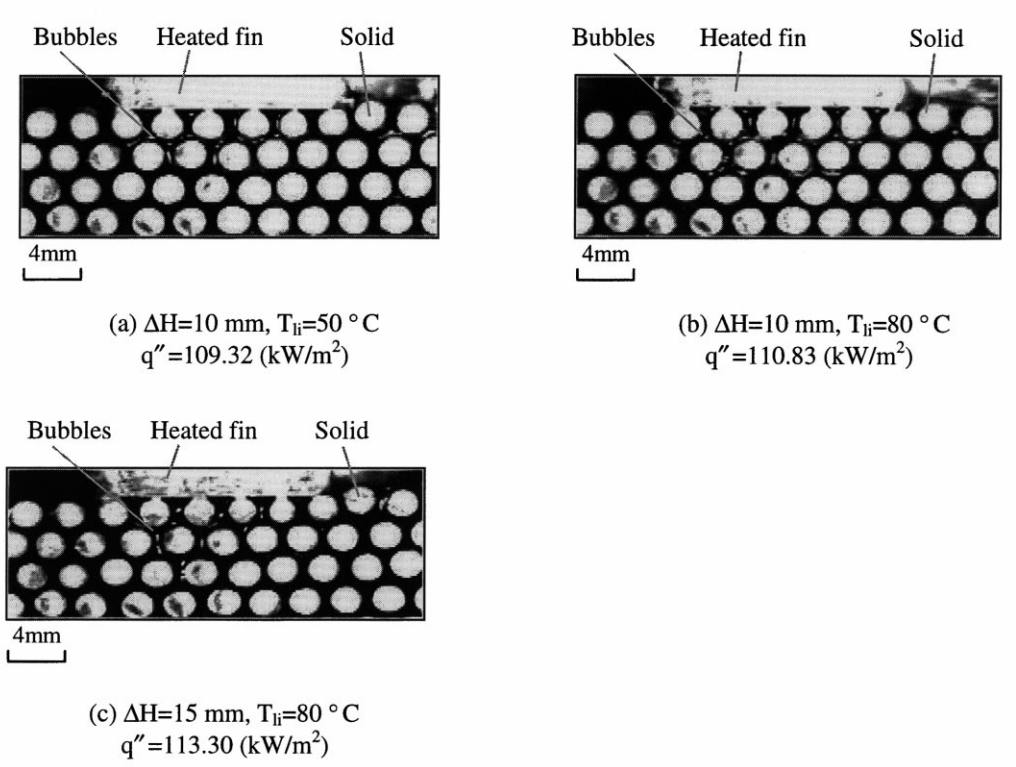

Fig. 12. Images of the two-phase zone below the heated surface for different inlet temperature and adverse hydrostatic head at the heat flux of 109.32–113.30 kW/m^2.

structure. Consequently, a higher inlet temperature of the subcooled liquid led to a higher heat transfer coefficient.

3.3. Effect of adverse hydrostatic head

Fig. 13(a) and (b) show that the influence of the adverse hydrostatic heads ($\Delta H = 10$ and 15 mm) on the heat transfer coefficient for the inlet temperatures of 50 and 80°C, respectively. It is seen that both the heat transfer coefficient and the critical heat flux increased with the decrease of the adverse hydrostatic head from 15 to 10 mm. This is mainly because the replenishment of liquid to the heated surface became more difficult as the water level was lowered. For the same reason, it can be speculated that both the heat transfer coefficient and the critical heat flux become very high as the adverse hydrostatic becomes zero or flushes with the heated surface. The visual images corresponding to these conditions are presented in Fig. 12(b) and (c). A comparison between the Fig. 12(b) and (c) shows that the two-phase zone for $\Delta H = 10$ mm was thinner in the vertical direction than for $\Delta H = 15$ mm at almost the same heat flux. This is because for a larger adverse hydrostatic head (or a larger distance between the heated surface and the water level in the water level container), bubbles mostly migrated downward due to the lower pressure in the vicinity of the heated surface. On the other hand, for a smaller adverse hydrostatic head, most of the bubbles moved laterally toward the vapor grooves due to the higher hydrostatic pressure from the water container. It is evident from Fig. 12(b) and (c) that for the smaller hydrostatic head, the two-phase zone is wider in the horizontal direction than that for the larger hydrostatic head. Therefore, a wider two-phase zone lead to a larger evaporation surface, thereby the heat transfer is enhanced for a smaller hydrostatic head.

4. Conclusions

A visual experiment on the phase-change behaviors in a vertical two-dimensional porous structure consisting of staggered miniature silver–copper circular cylinders was performed. Photographic results of this study lead to the following conclusions:

1. For a small or moderate heat flux, a co-existing

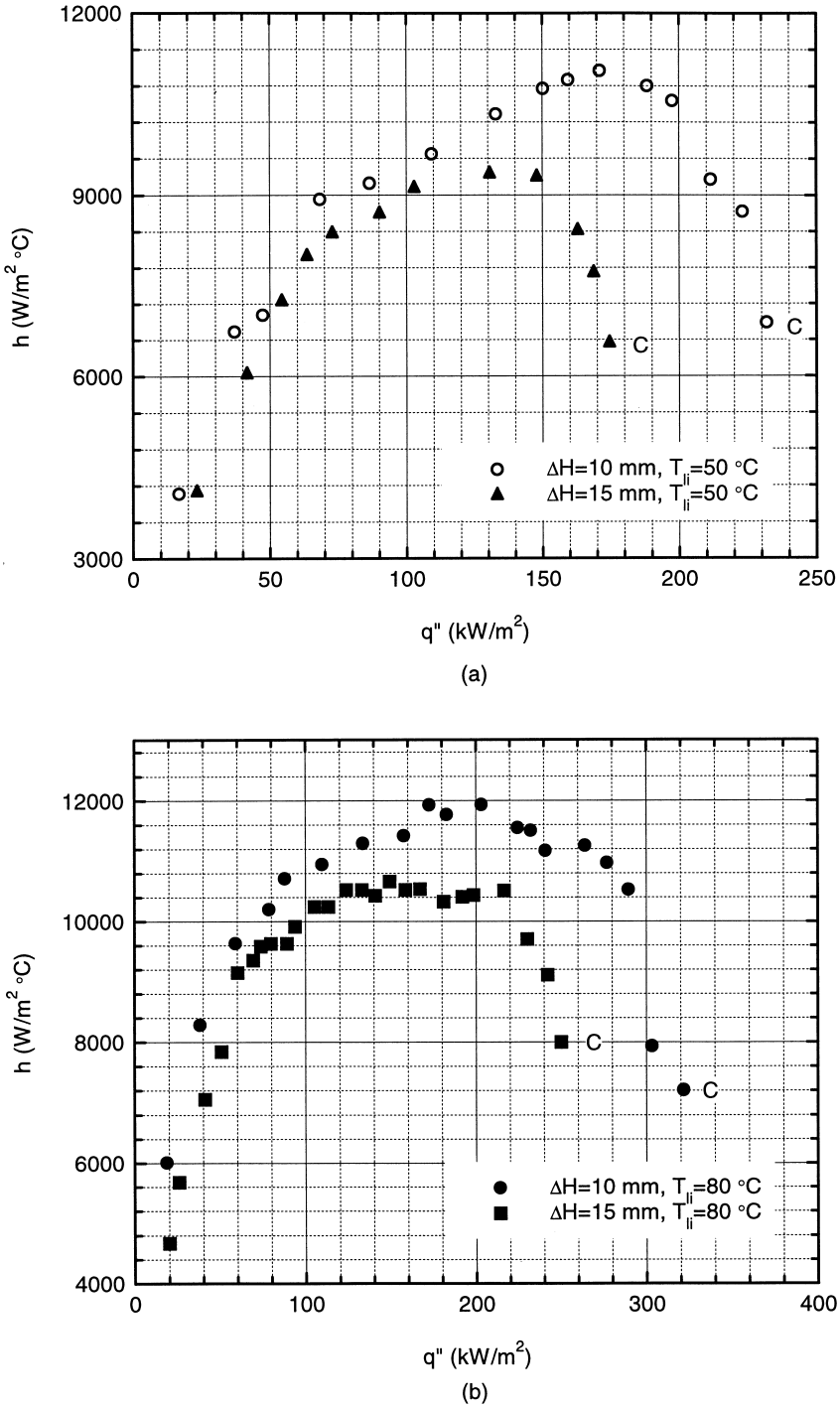

Fig. 13. Effect of the adverse hydrostatic head on the heat transfer coefficient at $T_{li} = 50$ and 80°C (where 'C' represents the critical heat flux point).

zone of bubbles and liquid existed in the porous structure adjacent to the heated surface; this two-phase zone expanded laterally and shrank vertically as the imposed heat flux was increased. Correspondingly, the heat transfer coefficient increased with the increase of heat flux until a peak value occurred.

2. When the imposed heat flux was further increased, the primary bubbles coalesced immediately once they were generated from the heated surface. The existence of the coalesced bubbles beneath the heated surface caused an increase in the thermal resistance. Therefore, the heat transfer coefficient decreased. Once the heat flux exceeded the critical heat flux, a stable vapor film formed underneath the heated surface and a further heat addition resulted in a rapid increase of the temperatures both in the heating block and in the vapor exit.
3. The reason why both the heat transfer coefficient and the critical heat flux increased with the increase of the inlet fluid temperature is because a higher inlet temperature led to a wider two-phase zone adjacent to the horizontal heated surface.
4. A higher adverse hydrostatic head led to both a lower heat transfer coefficient and a lower critical heat flux. This is mainly because replenishment of liquid to the heated surface became more difficult for a larger adverse hydrostatic head.

Acknowledgements

This work was supported by Hong Kong RGC Earmarked Research Grant No. HKUST 809/96E.

References

[1] C.Y. Wang, P. Cheng, Multiphase flow and heat transfer in porous media, in: J.P. Hartnet, T.F. Irvine, Y.I. Cho, G.A. Greene (Eds.), Advances in Heat Transfer, vol. 30, Academic Press, New York, 1997, pp. 93–196.

[2] R.J. Raiff, P.C. Wayner Jr, Evaporation from a porous flow control element on a porous heat source, International Journal of Heat and Mass Transfer 16 (10) (1973) 1919–1929.

[3] K.T. Feldman, D.L. Noreen, Design of heat pipe cooled laser mirrors with an inverted meniscus evaporator wick, AIAA Paper 92-0148, 1980.

[4] S.V. Kovalev, S.L. Solovev, Heat transfer and hydrodynamics in the inverted meniscus evaporator of a heat pipe, in: Proceedings of the Sixth International Heat Pipe Conference, Grenoble, France, 1987, pp. 116–120.

[5] D. Khrustalev, A. Faghri, Heat transfer in the inverted meniscus type evaporator at high heat fluxes, International Journal of Heat and Mass Transfer 38 (16) (1995) 3091–3101.

[6] A. Faghri, Heat Pipe Science and Technology, Taylor and Francis, Washington DC, 1995.

[7] J.T. Dickey, G.P. Peterson, Experimental and analytical investigation of a capillary pumped loop, Journal of Thermophysics and Heat Transfer 8 (3) (1994) 602–607.

[8] J. Ku, Overview of capillary pumped loop technology, in: Proceedings of the Twenty Ninth National Heat Transfer Conference, HTD-Vol. 236, Atlanta, GA, 1993, pp. 1–17.

[9] H. Wulz, E. Embacher Capillary pumped loops for space applications: experimental and theoretical studies on the performance of capillary evaporator designs, in: Proceedings of AIAA/ASME Fifth Joint Thermophysical and Heat Transfer Conference., Seattle, WA, 1990, AIAA-90-1739.

[10] Y. Cao, A. Faghri, Analytical solution of flow and heat transfer in a porous structure with partial heating and evaporation on the upper surface, International Journal of Heat and Mass Transfer 37 (10) (1994) 1525–1533.

[11] Y. Cao, A. Faghri, Conjugate analysis of a flat-plate evaporator for capillary loops with three-dimensional vapor flow in the groove, International Journal of Heat and Mass Transfer 37 (3) (1994) 401–409.

[12] A.S. Demidov, E.S. Yatsenko, Investigation of heat and mass transfer in the evaporation zone of a heat pipe operating by the 'inverted meniscus' principle, International Journal of Heat and Mass Transfer 37 (14) (1994) 2155–2163.

[13] Q. Deng, T. Ma, Z. Zhang, J. Wang, Experimental investigation on the performance of evaporator for capillary pumped loops, Journal of Engineering Thermophysics 19 (3) (1998) 330–334.

[14] Q. Liao, T.S. Zhao, Evaporative heat transfer in a capillary structure heated by a grooved block, Journal of Thermophysics and Heat Transfer 13 (1) (1999) 126–133.

[15] S.H. Anderson, C.J. Gantzer, J.M. Boone, R.J. Tully, Rapid nondestructive bulk density and soil–water content determination by computed tomography, Soil Science Society American Journal 52 (1988) 35–40.

[16] J. Jasti, G. Hesion, L. Geldkamp, Microscopic imaging of porous media using X-Ray computer tomography, in: Proceedings of the Sixty Fifth Annual Technical Conference and Exhibition of the Society of Petroleum Engineers, New Orleans, Los Angles, 1990, pp. 23–26.

[17] M.D. Shattuck, R. Behringer, Onset and stability of convection in porous media: visualization by magnetic resonance imaging, Physical Review Letters 75 (10) (1995) 1934–1937.

[18] W. Daily, A. Ramirez, Evaluation of electromagnetic tomography to map in situ water in heated welded tuff, Water Resources Research 25 (1989) 1083–1096.

[19] V.R. Latorre, H.D Glen, Microwave measurements of water content of bentonite, in: Proceedings of the Second Annual International High Level Radioactive Waste Management Conference, American Nuclear Society. Las Vegas, 1991.

[20] S.J. Kline, F.A. McClintock, Describing uncertainties in single-sample experiments, Mechanical Engineering, January 1953, pp. 3–12.